Inorg. Chem. **2007**, *46*, 8478–8480

Weak Ferromagnetism in a Semiconducting (Ethylenedithiodiselenadithiafulvalenoquinone-1,3-diselenolemethide)$_2$·$FeBr_4$ Salt

Toshiki Hayashi,[†,‡] Xunwen Xiao,[†,§] Hideki Fujiwara,*[,†,§] Toyonari Sugimoto,*[,†,§] Hiroyuki Nakazumi,[‡] Satoru Noguchi,*[,§,||] and Hiroko Aruga Katori[⊥]

Department of Chemistry, Osaka Prefecture University, Osaka 599-8570, Japan, CREST, Japan Science and Technology Agency, Saitama 332-0012, Japan, Department of Applied Chemistry, Osaka Prefecture University, Osaka 599-8531, Japan, Department of Physics and Electronics, Osaka Prefecture University, Osaka 599-8531, Japan, and RIKEN (The Institute of Physical and Chemical Research), Saitama 351-0198, Japan

Received June 27, 2007

The 2:1 salts of a new bent donor molecule, ethylenedithiodiselenadithiafulvalenoquinone-1,3-diselenolemethide (EDT-DSDTFVODS) and either an $FeBr_4^-$ or a $GaBr_4^-$ ion exhibit semiconducting properties and had small activation energies. The Fe^{III} d spins of the $FeBr_4^-$ salt are initially subject to a strong antiferromagnetic interaction and afterward exhibited a weak ferromagnetism at 3.8 K with a very small remanent magnetization of ca. 4×10^{-2} μ_B and a spin-flop near 25 kOe along the intercolumnar direction.

Spintronics based on the relationship between the electron charge and spin states are expected to play an important role in the development of next-generation electronic devices.[1] These new electronics utilize a magnetoresistance (MR) effect in which electrical resistance increases or decreases when a magnetic field is applied. Several MR effects are already known, but recently a tunneling MR effect has attracted much attention because it may aid in the development of a spintronics device with improved data density, S/N ratio, response time, and required magnetic field.[2] This MR effect depends on a ferromagnetic metal or semiconductor in which a current of electrons is spin-polarized and furnished with two components of charge and spin. Because such materials already exist in metallic and inorganic systems, many current efforts aim to develop spintronics devices that use the materials as source and drain electrodes and also as a carrier layer. On the other hand, corresponding organic materials have not yet been identified and the tunneling MR effect has not been investigated in an organic system.

Our recent efforts have been directed toward generating an unprecedented ferromagnetic molecular metal or semiconductor by using charge-transfer (CT) salts created with new donor molecules synthesized in our laboratory, such as tetrathiafulvalenoquinone(-thioquinone)-1,3-dithiolemethide and its derivatives, and magnetic $FeCl_4^-$ or $FeBr_4^-$ ions.[3] Very recently, a 2:1 CT salt of ethyelenedithiodiselenadithiafulvalenothioquinone-1,3-diselenolemethide (EDT-DSDTFVSDS, **1**) and $FeBr_4^-$ ion (**1**$_2$·$FeBr_4$) was found to exhibit metallic conductivity down to 0.6 K and to show antiferromagnetic ordering of the $FeBr_4^-$ ions' Fe^{III} d spins at 3.3 K. This temperature is the highest so far at which this behavior has been observed, and it occurred because of a strong interaction with the conducting π electrons.[3e] Nevertheless, ferromagnetic ordering has still not been achieved.

In this study, **1** was converted to the corresponding ketone derivative (EDT-DSDTFVODS, **2**), which also generated a 2:1 CT salt with the $FeBr_4^-$ ion (**2**$_2$·$FeBr_4$). We report that this $FeBr_4^-$ salt was a semiconductor, but when the Fe^{III} d spins strongly antiferromagnetically interacted with each other, the $FeBr_4^-$ salt exhibited weak ferromagnetism at 3.8 K.

* To whom correspondence should be addressed. E-mail: hfuji@c.s.osakafu-u.ac.jp (H.F.), toyonari@c.s.osakafu-u.ac.jp (T.S.), noguchi@pe.osakafu-u.ac.jp (S.N.).

† Department of Chemistry, Osaka Prefecture University.

‡ Department of Applied Chemistry, Osaka Prefecture University.

§ CREST, Japan Science and Technology Agency.

|| Department of Physics and Electronics, Osaka Prefecture University.

⊥ RIKEN.

(1) Žutić, I.; Fabian, J.; Das Sarma, S. *Rev. Mod. Phys.* **2004**, *76*, 323−410.

(2) (a) Julliere, M. *Phys. Lett. A* **1975**, *54A*, 225−226. (b) Miyazaki, T.; Tezuka, N. *J. Mag. Magn. Mater.* **1995**, *139*, L231−L234. (c) Yuasa, S.; Nagahama, T.; Fukushima, A.; Suzuki, Y.; Ando, K. *Nat. Mater.* **2004**, *3*, 868−871.

(3) (a) Matsumoto, T.; Kominami, T.; Ueda, K.; Sugimoto, T.; Tada, T.; Noguchi, S.; Yoshino, H.; Murata, K.; Shiro, M.; Negishi, E.; Toyota, N.; Endo, S.; Takahashi, K. *Inorg. Chem.* **2002**, *41*, 4763−4769. (b) Noguchi, S.; Matsumoto, A.; Matsumoto, T.; Sugimoto, T.; Ishida, T. *Physica B* **2004**, *346*−*347*, 397−401. (c) Matsumoto, T.; Sugimoto, T.; Aruga-Katori, H.; Noguchi, S.; Ishida, T. *Inorg. Chem.* **2004**, *43*, 3780−3782. (d) Fujiwara, H.; Wada, K.; Hiraoka, T.; Hayashi, T.; Sugimoto, T.; Nakazumi, H.; Yokogawa, K.; Teramura, M.; Yasuzuka, S.; Murata, K.; Mori, T. *J. Am. Chem. Soc.* **2005**, *127*, 14166−14167. (e) Hayashi, T.; Xiao, X.; Fujiwara, H.; Sugimoto, T.; Nakazumi, H.; Noguchi, S.; Fujimoto, T.; Yasuzuka, S.; Yoshino, H.; Murata, K.; Mori, T.; Aruga-Katori, H. *J. Am. Chem. Soc.* **2006**, *128*, 11746−11747. (f) Fujiwara, H.; Hayashi, T.; Sugimoto, T.; Nakazumi, H.; Noguchi, S.; Li, L.; Yokogawa, K.; Yasuzuka, S.; Murata, K.; Mori, T. *Inorg. Chem.* **2006**, *45*, 5712−5714.

10.1021/ic701260p CCC: $37.00
Published on Web 09/12/2007

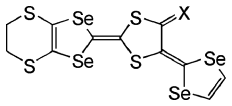

X = S: **EDT-DSDTFVSDS, 1**
X = O: **EDT-DSDTFVODS, 2**

Compound **1** was reacted with 6 equiv of mercury(II) acetate in acetic acid/THF (1:5, v/v) and then was recrystallized from CS_2/hexane to generate **2** as a red powder [mp 207−208 °C (dec)] with a 90% yield. The chlorobenzene/ethanol (9:1, v/v) solution of **2** and $(n\text{-Bu})_4N{\cdot}FeBr_4$ or $(n\text{-Bu})_4N{\cdot}GaBr_4$ was exposed to electrochemical oxidation at 45 °C with a constant current of 0.2 μA to generate black crystals of $\mathbf{2}_2{\cdot}FeBr_4$[4] and $\mathbf{2}_2{\cdot}GaBr_4$[5] after several weeks.

Figure 1a shows a crystal structure projection of $\mathbf{2}_2{\cdot}FeBr_4$ in the *ac* plane. Almost the same crystal structure was obtained for $\mathbf{2}_2{\cdot}GaBr_4$. Two crystallographically independent **2** molecules (**A** in a neutral state and **B** in a cation radical state, respectively, judging from their bond lengths) appear in the crystal (Figure 1a), and the two molecules are stacked in a sequence of −**ABB′A′**− along the *a* axis to form one-dimensional columns. The top and side views of the overlaps between **A** and **A′** (**A**/**A′**), between **A** and **B** (**A**/**B**), and between **B** and **B′** (**B**/**B′**) in each column are shown in Figure 1b. Obviously, the orbital overlaps are more extensive in the order of **B**/**B′** > **A**/**B** > **A**/**A′**, although the interplanar distances are almost the same (3.56, 3.57, and 3.55 Å). As discussed below, the molecular orbital (MO) calculations showed an increase in the overlap integrals ($S_{\pi\pi}$) in the order of **B**/**B′** >> **A**/**B** > **A**/**A′**. Consequently, a set of **A**, **B**, **B′**, and **A′** form a tetramer, and the tetramers are repeatedly stacked in each column. Because this salt is composed of two donor molecules and one $FeBr_4^-$ ion, each tetramer occupies two positive charges and two spins. The two spins residing in each tetramer are likely placed preferentially at the two **B** molecules to form a singlet state. In addition, neighboring columns have large overlaps with each other to make up the donor layers in the *ab* plane (Figure 1b). $FeBr_4^-$ ions are located between neighboring donor layers and arranged with a distorted honeycomb structure. Br···Br contacts with short distances (4.03 and 4.67 Å) exist between neighboring $FeBr_4^-$ ions. Furthermore, neighboring $FeBr_4^-$ ions have contacts with donor molecules in the neighborhood, as can be seen from the Br···S (3.78 and 3.90 Å) and Br···Se (3.56, 3.74, 3.75, and 3.91 Å) contact distances.

As is expected from the stacking structure of donor molecules, electrical conductivities of the $FeBr_4^-$ and $GaBr_4^-$ salts at room temperature were moderate (ca. 0.1 S cm^{-1}).

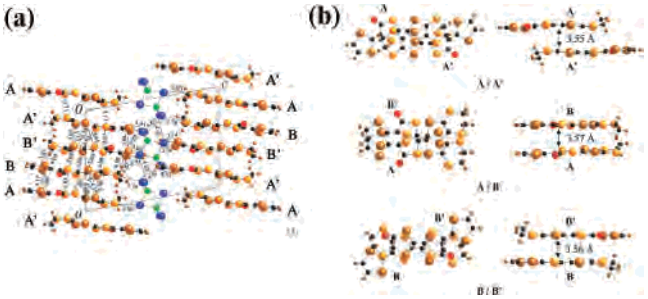

Figure 1. Crystal structure of $\mathbf{2}_2{\cdot}FeBr_4$: (a) a side view; (b) overlaps between neighboring donor molecules (**A**/**A′**, **A**/**B**, and **B**/**B′**)

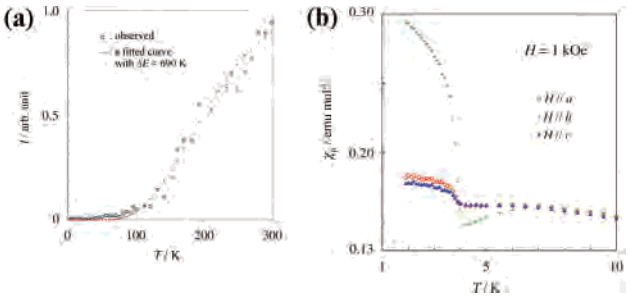

Figure 2. Temperature (T) dependences of (a) the ESR signal intensity (I) for $\mathbf{2}_2{\cdot}GaBr_4$ in the T range of 4−300 K and of (b) paramagnetic susceptibility (χ_p) for single crystals of $\mathbf{2}_2{\cdot}FeBr_4$ in the T range of 1.9−10 K. H is applied to each of the *a*, *b*, and *c* axes.

Their conducting behavior became semiconducting with small activation energies of 50−70 meV. The $FeBr_4^-$ salt exhibited very interesting magnetic properties. The temperature (T) dependence of paramagnetic susceptibility (χ_p) was measured using the polycrystals under a magnetic field (H) of 1 kOe in the T range of 1.9−300 K. Above 20 K, the χ_p values obeyed the Curie−Weiss law and exhibited a Curie constant of 4.43 emu K mol^{-1} and a Weiss temperature of −15.5 K. The Curie constant observed is close to the value (4.38 emu K mol^{-1}) calculated for the Fe^{III} ($S = {}^5/_2$) spin entity. The large negative Weiss temperature indicates a strong antiferromagnetic interaction between the d spins of $FeBr_4^-$ ions. Below 20 K, χ_p gradually became smaller than the value expected based on the Curie−Weiss curve, reached a maximum near 7 K, and then slightly decreased with decreasing T but abruptly increased near 4 K. This χ_p−T behavior suggests a low-dimensional antiferromagnetic ordering near 7 K and a three-dimensional magnetic ordering accompanied by a remanent magnetization near 4 K. The donor molecules' π spins do not contribute to the magnetization (M) but can interact somewhat with the d spins of the $FeBr_4^-$ ions because the two spins in each tetramer of donor molecules are in a singlet state. The electron spin resonance (ESR) signal intensity (I) for the $GaBr_4^-$ salt[6] became almost zero near 80 K, and the I−T plot was well described by a singlet−triplet model with an energy difference (ΔE) of ca. 690 K in the T range of 4−300 K (Figure 2a).

To characterize the $FeBr_4^-$ salt's magnetic ordering in more detail and to elucidate a possible mechanism, the χ_p−T measurement was carried out below 10 K on single crystals by applying H to each crystal axis. Each χ_p−T plot for $H \| a$, $H \| b$, and $H \| c$, where H = 1 kOe, is shown in Figure 2b. The χ_p−T behavior along $H \| b$ is very similar to that of the

(4) Crystal data for $\mathbf{2}_2{\cdot}FeBr_4$: $C_{22}H_{12}O_2S_8Se_8FeBr_4$, M = 1571.96, monoclinic, a = 14.428(9) Å, b = 13.924(9) Å, c = 19.35(1) Å, β = 100.15(3)°, V = 3825(4) Å^3, T = 296 K, space group $P2_1/a$, Z = 4, μ(Mo Kα) = 12.659 cm^{-1}, 75 606 reflections measured (R_{int} = 0.108), 8740 unique, of which 5682 were used in all calculations [$F^2 > 2.00\sigma(F^2)$]. The final R and Rw were 0.038 and 0.053, respectively.

(5) Crystal data for $\mathbf{2}_2{\cdot}GaBr_4$: $C_{22}H_{12}O_2S_8Se_8GaBr_4$, M = 1585.83, monoclinic, a = 14.4459(5) Å, b = 13.9377(4) Å, c = 19.3784(6) Å, β = 100.1070(9)°, V = 3841.2(2) Å^3, T = 296 K, space group $P2_1/a$, Z = 4, μ(Mo Kα) = 12.933 cm^{-1}, 74 014 reflections measured (R_{int} = 0.129), 8694 unique, of which 4003 were used in all calculations [$F^2 > 2.00\sigma(F^2)$]. The final R and Rw were 0.037 and 0.046, respectively.

(6) The ESR spectrum of $\mathbf{2}_2{\cdot}GaBr_4$ showed one broad signal in the T range measured.

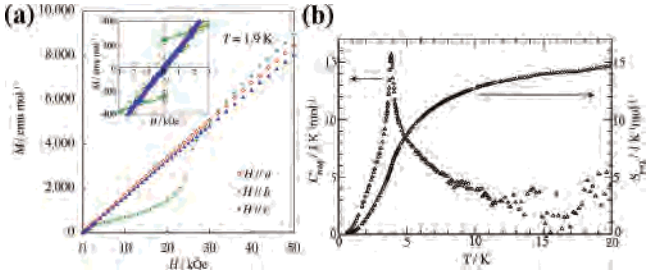

Figure 3. (a) Relationship between the magnetic field (H) and magnetization (M) for single crystals of $\mathbf{2}_2$·$FeBr_4$ when H is applied to each of the a, b, and c axes in the H range of 0 to +50 kOe at $T = 1.9$ K. The inset shows $M-H$ plots for $H\|a$, $H\|b$, and $H\|c$ in the H range of ±3 kOe. (b) Temperature dependence of the magnetic heat capacity (C_{mag}) and magnetic entropy (S_{mag}).

polycrystals. For $H\|a$ and $H\|c$, χ_p increased with decreasing T and showed a small jump near 4 K that was not preceded by a decrease. Figure 3a shows $M-H$ plots along $H\|a$, $H\|b$, and $H\|c$, where H ranges from 0 to +50 kOe at $T = 1.9$ K. Obviously, M increased almost linearly with H along $H\|a$ and $H\|c$. Meanwhile, a spin-flop occurred near 25 kOe in the $M-H$ plot along $H\|b$, and hysteresis with a remanent M value of ca. 4×10^{-2} μ_B (μ_B = Bohr magneton) and a coercive field of 380 Oe was observed in the lower H region (Figure 3a, inset). The heat capacities (C_{mol}) of $\mathbf{2}_2$·$FeBr_4$ and the corresponding $GaBr_4^-$ salt were also measured. The magnetic heat capacity (C_{mag}) of the $FeBr_4^-$ salt, calculated by subtracting the $GaBr_4^-$ salt's C_{mol} from the $FeBr_4^-$ salt's C_{mol}, showed a λ-shaped peak at 3.8 K (Figure 3b), which indicates its magnetic ordering temperature. The magnetic entropy (S_{mag}) of 14.8 J K^{-1} mol^{-1} calculated from C_{mag} is very close to R ln 6 (R = gas constant), or 14.89 J K^{-1} mol^{-1}, which is expected from the Fe^{III} ($S = {}^5/_2$) spin entity.

An extended Hückel MO method was used to calculate $S_{\pi\pi}$ between neighboring donor molecules, exchange integrals between d and d spins (J_{dd}), and exchange integrals between π and d spins ($J_{\pi d}$).[7] The $S_{\pi\pi}$ values between **A**/**A′** (a3), **A**/**B** (**B′**/**A′**) (a2), and **B**/**B′** (a1) overlaps in each donor-stacked column are -3.49×10^{-3}, -5.41×10^{-3}, and 27.14×10^{-3}, respectively, indicating that molecules of **A**, **B**, **B′**, and **A′** form a tetramer using stronger **A**/**B**, **B**/**B′**, and **B′**/**A′** overlaps instead of **A**/**A′** overlaps, even though **A**/**A′** molecules have close side-by-side overlaps ($b1 = -9.21 \times 10^{-3}$, $b2 = -9.53 \times 10^{-3}$, $p = -12.99 \times 10^{-3}$, $q = 2.72 \times 10^{-3}$, and $r = 0.94 \times 10^{-3}$) with donor molecules on neighboring columns. This result supports a singlet formation in each tetramer between two π spins, as mentioned above. On the other hand, for J_{dd} there are three different J_I (0.20 K), J_{II} (0.14 K), and J_{III} (0.007 K), while for $J_{\pi d}$, 12 different J_1-J_{12}'s exist with values of 4−0.02 K, which can also contribute to the magnetic ordering via their d spins.

The unique magnetic behavior of $\mathbf{2}_2$·$FeBr_4$ can be explained by the possible d-spin-driven spin structure of the $FeBr_4^-$ ions, shown in Figure 4. Above 20 K, the d spins are subject to a comparatively strong antiferromagnetic interaction with J_1 to form one-dimensional antiferromagnetic chains along the a axis. Upon a decrease in the temperature

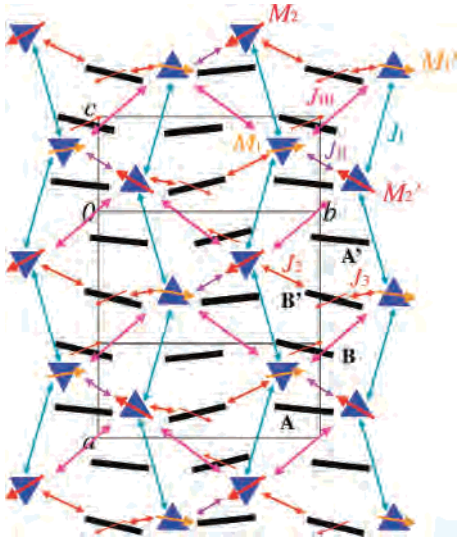

Figure 4. Spin structure of the $FeBr_4^-$ ions' d spins connected with J_I, J_{II}, J_{III}, J_2, and J_3. Each canted one-dimensional antiferromagnetic d-spin chain of $\cdots M_1M_2M_1M_2\cdots$ and its neighbor, ordered $\cdots M_2'M_1'M_2'M_1'\cdots$, has a reverse spin direction.

below 20 K, antiferromagnetic d chains begin to interact with each other through J_{II} and $J_{\pi d}$. The J_{II} interaction can arrange all d spins in an antiparallel manner, but two strong π−d interactions ($J_2 = 2.1$ K and $J_3 = 1.5$ K) between the d spins and the π spins on molecule **B** force the two interacting d spins into a parallel arrangement and destabilize the antiparallel spin structure. To relieve this situation, the spin structure that preferentially adopts a completely antiparallel arrangement must undergo some change. Consequently, a canted antiferromagnetism was used, after which a very small and anisotropic remanent M of ca. 4×10^{-2} μ_B mol^{-1} appeared. Judging from the fact that both the remanent M and the spin-flop are observed along the $H\|b$ direction, a spin structure as shown in Figure 4 is most likely. In this structure, a pair of neighboring d spins (M_1 and M_2) in each of the one-dimensional d-spin chains are almost directed toward the b axis and canted toward each other. Furthermore, when one d-spin chain has an arrangement of $\cdots M_1M_2M_1M_2\cdots$, its neighbor has an arrangement of $\cdots M_2'M_1'M_2'M_1'\cdots$, where M_1' and M_2' have a reverse spin direction relative to M_1 and M_2 along the b axis. The canting between the antiferromagnetically interacting M_1 and M_2 might occur by a spin frustration as mentioned above. Note that the present weak ferromagnetism is generated by a very unique arrangement of canted one-dimensional antiferromagnetic d-spin chains and neighboring d-spin chains with reverse spin directions.

Acknowledgment. The authors thank Professor Takehiko Mori for his kind advice in the MO calculations of overlap and spin exchange integrals.

Supporting Information Available: X-ray crystallographic files for $\mathbf{2}_2$·$FeBr_4$ and $\mathbf{2}_2$·$GaBr_4$ crystals in CIF format and $\pi-\pi$ overlap integrals and d−d exchange integrals calculated by an extended Hückel MO method for $\mathbf{2}_2$·$FeBr_4$. This material is available free of charge via the Internet at http://pubs.acs.org.

IC701260P

(7) Mori, T.; Katsuhara, M. *J. Phys. Soc. Jpn.* **2002**, *71*, 826−844.